

Convergence and accuracy of FDTD modelling for periodic plasmonic systems

L. RASSINFOSSE,¹ J. MÜLLER,¹ O. DEPARIS,²  S. SMEETS,³ G. ROSOLEN,³ AND S. LUCAS^{1,*} 

¹Laboratoire d'Analyse par Réactions Nucléaires (LARN), Namur Institute of Structured Matter (NISM), University of Namur, 61 Rue de Bruxelles, Namur B-5000, Belgium

²Laboratoire de Physique du Solide (LPS), Namur Institute of Structured Matter (NISM), University of Namur, 61 Rue de Bruxelles, Namur B-5000, Belgium

³Micro- and Nanophotonic Materials Group, Research Institute for Materials Science and Engineering, University of Mons, 20 place du Parc, Mons B-7000, Belgium

*stephane.lucas@unamur.be

Abstract: Despite the widespread use of the finite-difference time-domain (FDTD) method for modeling plasmonic systems, there is a lack of detailed convergence and accuracy studies for periodic nanoparticle systems in which both particle radius and interparticle distance are critical parameters. Using an in-house parallelized 3D-FDTD code for which we implemented interface field averaging, convergence and accuracy were evaluated for various spherical particle radii, inter-distances, and radius-to-mesh size ratios. We found that Interface Field Averaging (IFA) FDTD improved accuracy and convergence with respect to per-component (Per-C) meshing. In the worst case of this study, the convergence error decreased from 4.9% to 2.6% only by using IFA. Accuracy was verified by benchmarking our simulation results with COMSOL Multiphysics software. Furthermore, we notice that there exists no general rule for choosing the mesh size. Careful convergence testing should therefore be carried out systematically.

© 2024 Optica Publishing Group under the terms of the [Optica Open Access Publishing Agreement](#)

1. Introduction

Metallic nanoparticle (MNP) based structures continue to attract great interest within the scientific community for their applications in light-harvesting [1–3], sensing [4,5] or nonlinear optics [6,7]. MNPs are particularly interesting since many different experimental techniques can synthesize nanoparticles of various compositions and sizes [8]. Nevertheless, the resulting optical properties are very sensitive to geometry [9], including the interparticle distance [10] and, in multilayer systems, the spacer layer thickness [11–14]. Therefore, efficient simulation tools for the prediction of the optical response of MNP structures are desirable. Fortunately, the progress in both simulation techniques and computational power has enabled to carry on optimizations of plasmonic structures that were once too demanding in terms of computational resources. Among available methods [15], the Finite Element Method (FEM), the Finite-Difference Frequency-Domain (FDFD) method, the Rigorous Coupled Wave Analysis (RCWA) [16] and the Finite-Difference Time-Domain (FDTD) method are among the most popular ones to simulate the response of plasmonic structures. This article focuses on the FDTD method [17,18] and its efficiency for this purpose. Reviews and benchmarks of different methods can be found in [19–21].

Many current MNP-based designs utilize nanoparticles with a radius between 20 and 60 nm (Table 1) for applications within the ultraviolet - near infrared range (300–1250 nm). Few articles discuss the case of very small nanoparticles (i.e., radius around 10 nm). Some numerical studies using the FDTD method do not mention the mesh size, in spite of the fact that it is a crucial parameter for the accuracy of simulations.

Table 1. Brief overview of some recent MNP-based plasmonic designs by numerical simulations.

Reference	Radius of nanospheres (nm)	MNP material	Matrix material	Simulation method	Mesh size (nm)	Purpose
[22]	11	Au	Dichloromethane solution	FDTD	0.58	Evaluation of the number of MNPs in a solvent
[23]	25 - 50	Ag	Rhodamine 590 Chloride polymer	FDTD	Not mentioned	Modification of the emission
[24]	12 - 50	Ag	Air / Si	FDTD	4	Study of MNP synthesis
[25]	25 - 50	Au	Dielectric ($n \in [1,2]$)	FDFD	Not mentioned	Evaluation of the impact of the MNPs' orientation
[26]	40 - 90	Ag, Al, Au, SiO ₂ , TiO ₂ , Si ₃ N ₄	Aluminium doped Zinc Oxide (AZO)	FDTD	Not mentioned	Absorption enhancement for solar cells
[27]	50	Ag	Air	FEM	Not mentioned	Sensing applications
[28]	10-50	Ag	Glucose solution	FDTD	Not mentioned	Sensing applications
[29]	10-100	Au	Various solutions	FEM	Not mentioned	Dengue diagnosis
[30]	10	Au	Air and water	FDTD	0.5	Surface enhanced Raman spectroscopy sensing
[31]	8-72	Ag	Air	FDTD	0.125	Coloring metal surfaces

Optical modelling of small (sub-wavelength scale) structures is by no means trivial [32]. For the FDTD method, technical limitations arise when fine meshing is required. Indeed, by using explicit FDTD models, i.e. which are exempt from matrix solutions, computation time and memory usage scale as the fourth and the third powers of the inverse of the mesh size, respectively [33]. Increasing the mesh size, i.e. decreasing the spatial resolution, reduces this computational cost, but the FDTD method can then suffer from staircase discretization, especially when the geometry of the mesh does not match the geometry of the simulated structure. This issue is particularly critical when using structured meshes based on Yee-cells [34]. Structured meshes are defined by quadrilaterals in 2D and hexahedrons in 3D. Their connectivity is implicit hence the neighbors of each element should not be stored in memory, which is a computational advantage. More advanced FDTD implementations exist and recent works have demonstrated the feasibility of implementing 3D unstructured meshes for a FDTD code which addresses such discretization problems [35]. Regarding more advanced structured meshes, one can resort to graded meshes. Graded meshes consist in refining the mesh size in certain regions, such as near interfaces, in order to model the local field phenomena with more accuracy. Graded meshes are tedious to implement and will not necessarily solve computation time problems. Another possible method is the Interface Field Averaging (IFA) method [36–40]. IFA can be found in literature as “conformal-FDTD”, but to avoid any confusion with other interpretations of conformal meshing for which the mesh element boundaries must coincide with the object boundaries, we decided to rename the method. A review of the limitations of this method can be found in [41]. IFA, is easy to implement and assessing the benefits of this method is one of the goals of this work.

Whatever the method used, inappropriate meshing results in convergence issues. Even for commercial simulation software, such as Lumerical [42] which uses a state-of-the-art FDTD implementation, convergence testing is required when simulating metallic NPs [43]. A detailed 3-D convergence analysis, with regard to the mesh size, was reported in [44]. The case study consisted of an isolated metallic nanoparticle with a radius of 60 nm, a metal dipole antenna and a metal bowtie antenna. However, a parametric study of the convergence as a function of the mesh size for various spherical nanoparticle radii, including very small ones (radius < 10nm), as well as interacting MNPs, has not yet been addressed in literature. In this article, we investigate the influence of the mesh size on the convergence of the Reflectance, Transmittance and Absorptance (RTA) spectra for silver (Ag) NPs of radii varying between 5 nm and 60 nm, arranged periodically in a silicon carbide (SiC) host medium. We then examine the benefits and limitations of using IFA in this geometry. Finally, we compare our FDTD results with those obtained by FEM using unstructured mesh thanks to the COMSOL Multiphysics [45] software which performs very well for nanometric plasmonic structures [32,46]. Below a NP radius of 5 nm, the dielectric function of metals such as silver is no longer independent of the size of the nanoparticles [24,47]. For this reason, that case will not be examined in this article. The choice of SiC and Ag materials is motivated by applications of plasmonic nanostructures for functional coatings. The aim is to produce a wear-resistant plasmonic structure which benefits from silver's excellent, and well-known, plasmonic properties but also from silicon carbides excellent mechanical properties such as great hardness and good anti-oxidation properties.

2. Method

In this section, we will detail the geometry of the MNP system, describe the simulation parameters and explain how we evaluate the convergence of the RTA spectra.

2.1. Geometrical model

The optical modelling is performed with a home-made FDTD (Finite-Difference Time-Domain) code [48–50]. The code is developed in Fortran95, parallelized thanks to the openMP [51] library and compiled with the Intel Fortran compiler ifort. Figure 1 is a cross-section of the 3-dimensional model which is periodic in two directions (x,y). Periodic boundary conditions (PBC) are used to mimic an infinite periodic structure. A Convolutional Perfectly Matched Layer (CPML) absorbing medium is placed above and below the simulated structure. The CPML absorbing medium is highly absorptive for propagative and evanescent waves, which allows it to be placed near the structure. Moreover, the CPML technique is independent of the host material used, and can therefore be adapted to dispersive media [52]. In order to model both host (SiC) and MNP (Ag) dispersive media, we used the Auxiliary Differential Equation (ADE) technique which is based on an advanced multiple Drude-Lorentz model [53]. The dielectric function is of the form

$$\varepsilon(\omega) = \varepsilon_{\infty} + \varepsilon_D(\omega) + \sum_{p=1}^P \varepsilon_p(\omega), \quad (1)$$

where ε_{∞} is the permittivity at infinite frequency, $\varepsilon_D(\omega) = \frac{\omega_p^2}{i\gamma_D\omega - \omega^2}$ is the Drude dielectric function and $\varepsilon_p(\omega) = \frac{\Delta\varepsilon(\omega_p^2 - i\gamma_p'\omega)}{\omega_p^2 - 2i\omega\gamma_p - \omega^2}$ a modified Lorentz function ($\gamma_D, \omega_D, \Delta\varepsilon, \omega_p, \gamma_p, \gamma_p'$ are real valued fitting coefficients). The number of modified Lorentz functions (P) needed to accurately describe the permittivity is fixed by the user. The refractive indices of silicon carbide and silver were obtained from [54] and [55], respectively, and are available online [56]. The model parameters, according Eq. (1), of the materials are reported in Table 2.

The illumination is chosen at normal incidence thanks to an incident plane-wave source adapted to periodic conditions. The reflected and transmitted electromagnetic powers are computed by

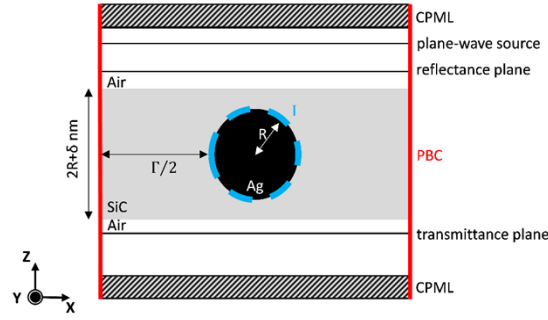


Fig. 1. Computational domain and material composition of the studied MNP system. $\delta = 10$ nm for all radii, Γ represents the interparticle distance, CPML = Convolutional Perfectly Matched Layer, PBC = Periodic Boundary Condition, I = Interface, which is where the field averaging will be applied and R = particle radius.

Table 2. Model parameters of SiC and Ag

Fitting coefficients	Ag		SiC		
ϵ_{∞}	1.6965		1.0513		
γ_D	3.2604e + 13		/		
ω_D	1.7205e + 32		0		
$\Delta\epsilon$	0.1000	1.8707	0.0100	3.8139	4.7918
ω_p	6.3052e + 15	7.7798e + 15	2.6301e + 15	7.6325e + 15	1.1124e + 16
γ_p	4.3146e + 14	2.9315e + 15	1.3008e + 15	1.9932e + 15	3.3752e + 15
γ'_p	1.8849e + 16	3.5490e + 15	2.5732e + 17	1.9209e + 03	7.3516e + 03

integrating the Poynting vector on two virtual planes, respectively above and below the structure. Due to the position of the reflectance plane, the incident field must be ignored while computing the Poynting vectors on this plane by using a total field/scattered field method. The absorptance A is computed according to the energy conservation relation $A = 1 - R - T$, where R and T are the reflectance and the transmittance, respectively. Finally, in an effort to compensate for staircase discretization errors in the spherical Ag MNPs, IFA is implemented. Its basic principle is simple: weighted averages of the electric field are computed if a mesh cell (Yee-cell) is crossed by an object (here a nanoparticle). Figure 2 illustrates a 2D example of a Yee-cell being crossed by an interface between two media. In this configuration, the horizontal segment at the cell's top edge on which $E_x(i + \frac{1}{2}, j + 1)$ is computed is completely within material 2 and needs no special considerations. On the contrary, the bottom segment where $E_x(i + \frac{1}{2}, j)$ crosses the boundary between material 1 and material 2. As a consequence, the electric field is computed by:

$$E_x\left(i + \frac{1}{2}, j\right) = \frac{\delta_x}{\Delta x} E_x^1\left(i + \frac{1}{2}, j\right) + \frac{1 - \delta_x}{\Delta x} E_x^2\left(i + \frac{1}{2}, j\right), \quad (2)$$

where E_x^1 and E_x^2 are computed as if they were completely inside material 1 and material 2, respectively.

2.2. Simulation parameters

Table 3 lists all the FDTD simulation parameters. The CPML thickness is fixed to 30 nm in order to avoid any reflection error. The distance between the CPML and the source, the distance

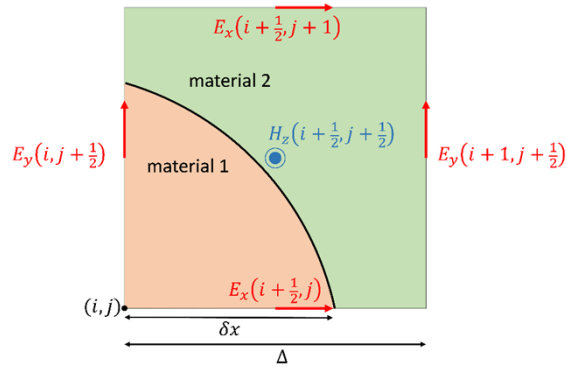


Fig. 2. 2D representation of the interface field averaging method. The indices “ i ” and “ j ” are taken along the two perpendicular periodic directions. Δ is the mesh size, i.e., the size of Yee-cell in the x direction.

between the source and the reflectance plane and the distance between the reflectance plane and the top surface of the structure are fixed to 5Δ , 10Δ and 10Δ , respectively, where Δ is the mesh size. The plane-wave is introduced by direct field in free space and the host material is SiC. The radius of the silver nanoparticles (R) varies between 5 and 60 nm. The edge-to-edge interparticle distance (Γ) between two adjacent nanoparticles is either 4 or 10 nm. The nanoparticle is placed at the center of the SiC slab in the periodic unit cell. Several mesh sizes are investigated: $R/5$, $R/10$, $R/20$, $R/40$, $R/50$, $R/60$, $R/100$ and $R/200$, R being the radius of the nanoparticles. Given a pulse duration of 2.7 fs, the simulation time is fixed to 25.0 fs in all cases in order to ensure a steady-state solution of the studied system. 25.0 fs is a choice based on the consideration that light travels in the simulation domain in approximately 0.5 fs. Once a steady-state solution is reached, further increasing the simulation time has no impact. The pulse duration was chosen short enough so that the spectral bandwidth of the pulse covers all the wavelengths of interest. The choice of closely packed periodically arranged spheres is motivated by the desire to maximize the numerical inaccuracies in case of bad meshing. This way, an appropriate meshing for periodically arranged spheres should also suit randomly distributed spheres with similar interparticle distances.

Concerning the FEM simulations with COMSOL, a Perfectly Match Layer (PML) absorbing medium of 750 nm is placed on the top and at the bottom of the stack. An unstructured tetrahedral mesh is used where the smallest element is in the interspace between particles and has a characteristic size of 0.66 nm. A mesh refinement study was done and dividing the mesh size by 2 implied a maximum difference of 0.15% in the calculated spectra.

The FEM simulations were computed with Intel Xeon E5-2643 v4 6 core 3.40 GHz CPUs. The FDTD simulations were computed with Intel Xeon E5-2660 8 core 2.20 GHz CPUs and AMD Epyc 7551P 32 core 2.0 GHz on a HPC cluster. For the FDTD simulations 2 CPUs per simulation were used. Table 4 and Table 5 summarize the computational costs for the FEM and FDTD simulations. Only the finest mesh simulation times are reported for the FDTD method. We plotted memory cost as a function of the error score (defined in next section) for the biggest and the smallest nanoparticle radius that was investigated and for an interparticle distance of 4 nm (Fig. 3).

Table 3. Summary of the simulation parameters

Parameter	Values
Radius, R (nm)	5, 10, 20, 40, 60
Interparticle distance, Γ (nm)	4, 10
Matrix material	SiC
Nanoparticle material	Ag
SiC thickness (nm)	$2R + 10$
Incident medium	Air
Emerging medium	Air
Simulation time (fs)	25
Pulse duration (fs)	2.7
CPML (nm)	30
Mesh size, Δ (nm)	R/5, R/10, R/20, R/40, R/50, R/60, R/100, R/200
Source type	Plane-wave
Distance CPML - source (nm)	5Δ
Distance reflectance plane - source (nm)	10Δ
Distance reflectance plane - structure (nm)	10Δ

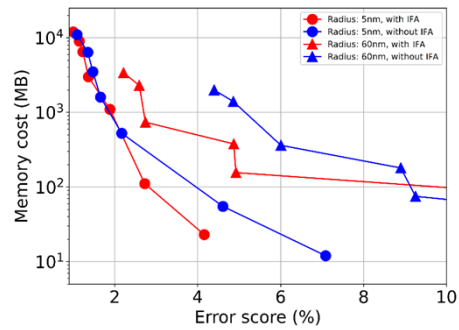


Fig. 3. Memory cost (in MB) as a function of the error score for 5 nm and 60 nm radius nanoparticles with an interdistance of 4 nm. Each data point represents a different mesh size and the error score was calculated with the COMSOL simulation as reference.

Table 4. FEM computation costs

Interparticle Distance (nm)	Nanoparticle radius (nm)	Time (min)	Memory Cost (GB)
4	5	1066	55
	10	753	44
	20	570	36
	40	492	33
	60	445	32
10	5	1559	75
	10	1003	54
	20	807	45
	40	628	39
	60	538	36

2.3. Performance metrics

2.3.1. Convergence metric

A common problem in convergence testing with complex structures is that the correct result is unknown. In order to evaluate convergence in simulations, we define a mesh size dependent error as:

$$\epsilon_{\lambda,\Delta}^Q = |Q_{\lambda,\Delta} - Q_{\lambda,\text{ref}}|$$

where $Q_{\lambda,\Delta}$ is the quantity of interest (reflectance, transmittance or absorptance) at wavelength λ and mesh size Δ . The subscript “ref” stands for a reference simulation. In the following, the reference simulation is either the FDTD simulation computed with the finest mesh (R/100 for 5-, 10- and 20-nm radius nanoparticles and R/200 for 40- and 60-nm radius nanoparticles) or the FEM simulations (COMSOL).

Table 5. FDTD computation costs

Interparticle Distance (nm)	Nanoparticle radius (nm)	Time (min)	Time (min)	Memory Cost (GB)	Memory Cost (GB)
		With IFA	Without IFA	With IFA	Without IFA
4	5	4137	3384	12	11
	10	2610	3775	9.4	5.2
	20	955	1357	5.8	3.3
	40	448	335	4.1	2.4
	60	218	345	3.4	2.0
10	5	6598	5498	25	23
	10	1451	1922	15	8
	20	563	836	7.5	4.2
	40	132	122	4.7	2.7
	60	85	89	3.9	2.3

Then, we defined a convergence error score (S) by arithmetic averaging ($\langle \dots \rangle$) the three quantities:

$$S_{\Delta} = \frac{1}{3} \left\langle \epsilon_{\lambda,\Delta}^R + \epsilon_{\lambda,\Delta}^T + \epsilon_{\lambda,\Delta}^A \right\rangle \quad (3)$$

Given that the spectra are normalized, S_{Δ} is directly interpretable as a relative value.

2.3.2. IFA improvement metric

In order to investigate the impact of IFA on convergence, we defined a IFA enhancement factor F_{Δ}^{IFA} as:

$$F_{\Delta}^{\text{IFA}} = \frac{S_{\Delta}^{\text{Per-C}} - S_{\Delta}^{\text{IFA}}}{S_{\Delta}^{\text{Per-C}}} \quad (4)$$

where $S_{\Delta}^{\text{Per-C}}$ and S_{Δ}^{IFA} are calculated using FEM simulation as common reference. If F_{Δ}^{IFA} is positive, then the convergence is improved by the IFA. If it is negative, then the IFA performs worse than the Per-C FDTD-implementation. Per-C meshing consists in assigning a permittivity $\epsilon_r(\omega, r)$ to each component of the electric field (E_x, E_y, E_z). Per-C meshing is already an improved meshing technique compared to uniform meshing; where E_x, E_y and E_z of one Yee-cell all have identical permittivities. A comparison of Per-C versus uniform meshes can be found in [44].

3. Results

One of the most important parameters in FDTD simulations is the mesh size. In this section, we analyze the convergence of reflectance, transmittance and absorptance spectra as function of the mesh size and the interparticle distance for radii varying between 5 and 60 nm. All the other simulation parameters given in Table 3 are kept constant. First, the overall convergence will be discussed. Then, the benefits of the IFA will be examined. Finally, for validation purposes, the results will be confronted to FEM simulations realized with COMSOL.

3.1. Per-component mesh convergence

The error score was computed using Eq. (3) with a Per-C mesh FDTD simulation with the finest grid as reference, for 4 and 10 nm particle inter-distances (Fig. 4(a), 4(d)). The error score is plotted on a logarithmic scale, as function of the mesh size for various sphere radii. The RTA spectra for the $R = 40$ nm particle radius and various mesh sizes are compared to those obtained with the finest mesh (reference), and their differences are plotted (Fig. 4(b), 4(c), 4(e), 4(f)).

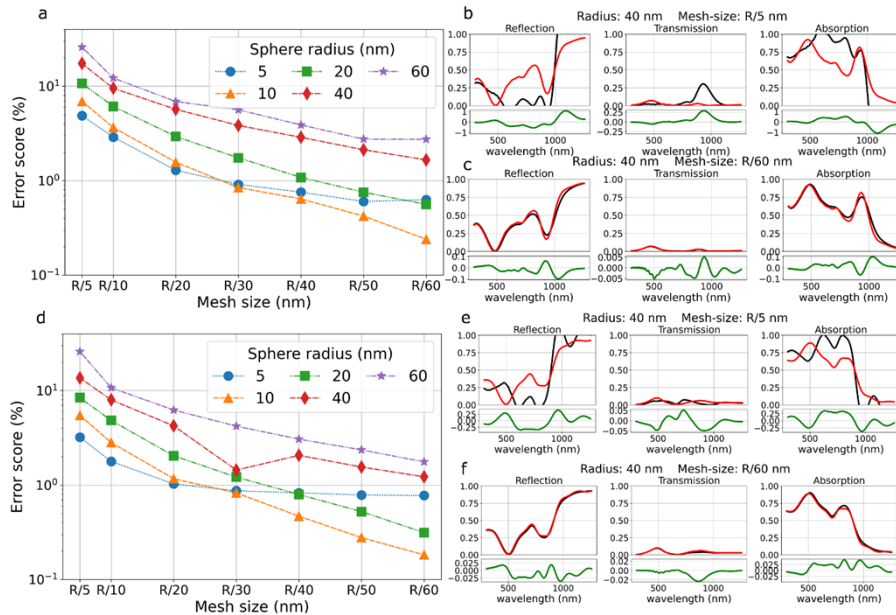


Fig. 4. Error score as function of the mesh size for an interparticle distance of 4 nm (a) and 10 nm (d). RTA spectra (in black) for a radius of 40 nm, an interparticle distance of 4 nm and a mesh size of R/5 nm (b) and R/60 nm (c). The red curves correspond to the R/200 simulation (taken as reference) and the green curves to the difference between red and black curves. (e) and (f) show the same simulations as (b) and (c) but for an interparticle distance of 10 nm.

From Fig. 4(b), it appears that a mesh size of R/5 is too coarse. For a 40-nm radius particle, the error score is 13.7% (Fig. 4(a)) and many resonance artifacts are present (compare black and red curves in Fig. 4(b)). For a mesh size of R/60, however, these unphysical resonances have disappeared (Fig. 4(c)) and the error score is reduced to 1.6% (Fig. 4(a)). There is no absolute rule concerning the convergence. An important criterion is that the simulation has to reflect the physical reality. Thus, the number of resonance peaks and their positions are among the factors that matter the most. Based on that, it appears from examination of Fig. 5 that the convergence is acceptable when the error score is close or below 1.0%. Once that level is reached, further reducing the mesh size slightly improves the convergence, but greatly increases the memory usage

and the computation time. Caution needs to be taken concerning the convergence for the largest spheres nevertheless. For a nanoparticle radius of 60 nm, a mesh size of R/60 and an interparticle distance of 4 nm the error score is 2.7% (Fig. 4(a)) and the simulations do not converge. This is because the small interparticle distance results in an intense electric field gradient in the gap between the nanoparticles, and a spatial resolution of 1 nm is too coarse to reliably describe the electric field within a gap of 4 nm. By contrast, error score is much lower (1.8%) for a larger gap, i.e. 10 nm (Fig. 4(d)). This confirms the hypothesis that insufficient spatial resolution of a sharp electric field gradient between nanoparticles leads to poor convergence. For a nanoparticle radius of 40 nm, an interparticle distance of 10 nm and a mesh size of R/60 the error score is 1.2% (Fig. 4(d)) and only minor differences with the R/200-mesh “reference” simulation are present (Fig. 4(f)), the convergence can therefore also be labeled as acceptable.

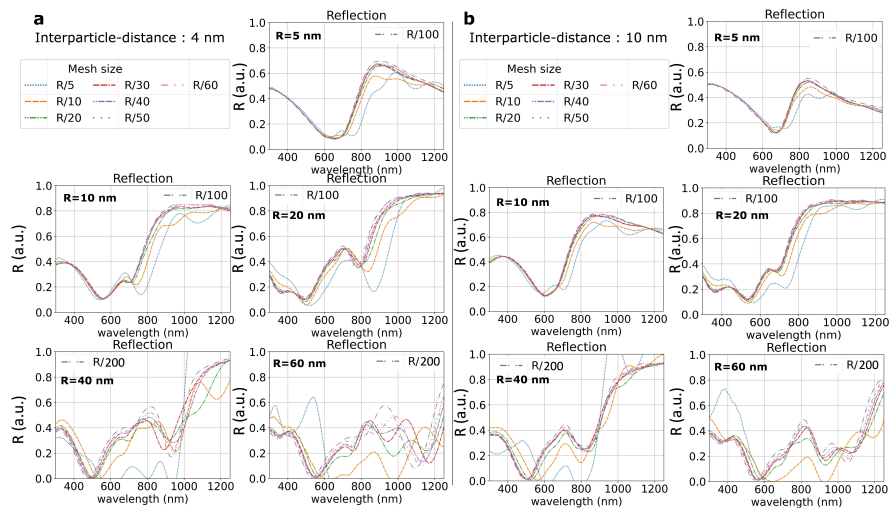


Fig. 5. Reflection spectra for all mesh sizes and all radii for an interparticle-distance of 4 nm (a) and 10 nm (b).

3.2. IFA convergence

The convergence with and without the IFA method is assessed through the calculation of the IFA enhancement factor computed with Eq. (4) and multiplied by 100 to be expressed as a percentage. In order to evaluate the convergence with a common reference, the FEM simulation was taken as reference. In most cases, IFA effectively improves the convergence of the simulations (Fig. 6). The enhancement factor is bigger for larger nanoparticles (i.e. 60 and 40 nm) owing to the increasing ratio between the nanoparticle radius and the fixed interparticle distance. The larger the particle, the larger the reflection upon the surface of the nanoparticle. Therefore, a finer description of this interface, as it is achieved by IFA, leads to a better convergence. For smaller nanoparticles, it is essentially the interaction in between the NPs that dominates and thus IFA has less impact. For both interparticle distances of 4 and 10 nm, a decrease in the enhancement factor can be noticed for smaller mesh sizes. At some point, the mesh is small enough so that IFA does not provide any major convergence enhancement, in that case F_{Δ}^{IFA} is close to zero. Overall, the IFA enhancement factor is higher for smaller interparticle distances. These results are a clear indication that choosing appropriate meshing for simulations, i.e., with plasmonic nanoparticle systems, requires fine particle discretization [44] and high interparticle spatial resolution [10]. The results also suggest that IFA could help improve the convergence of closely packed randomly

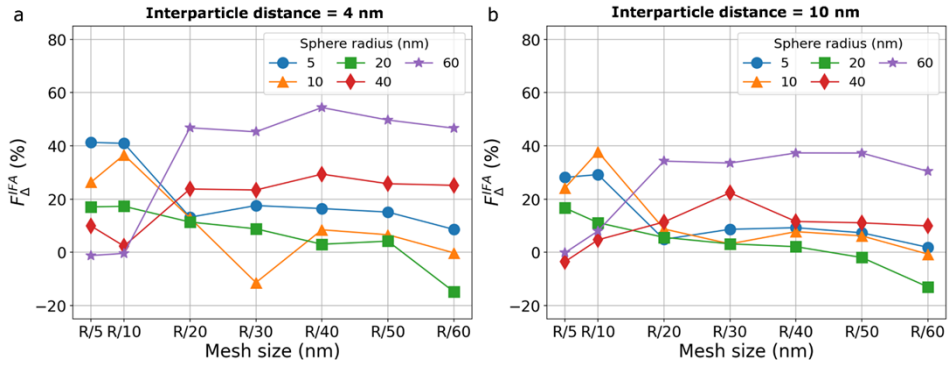


Fig. 6. Impact of the IFA on the convergence for an interparticle distance of 4 nm (a) and 10 nm (b). Positive values of F_{Δ}^{IFA} signify that IFA improves the convergence with respect to Per-C meshing.

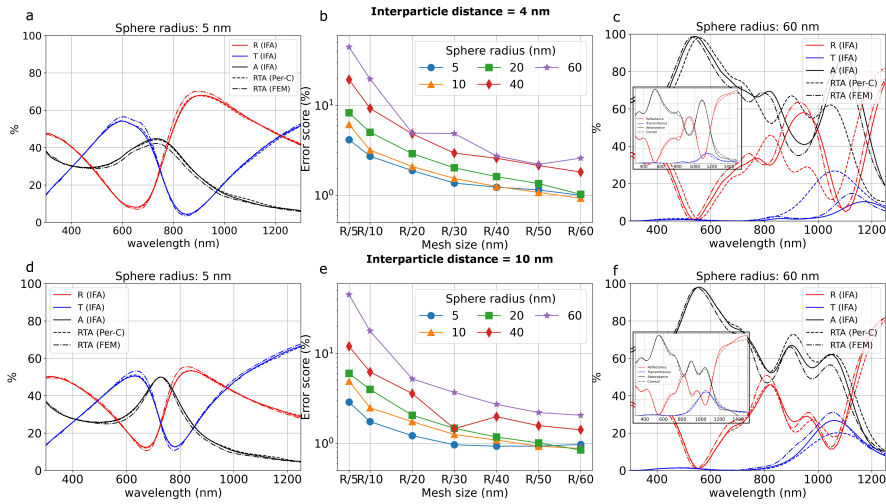


Fig. 7. RTA spectra simulated by FDTD with IFA (solid lines) and Per-C (dashed lines) meshes and by FEM (dash-dotted lines). Spectra (a) and (c) were computed with spheres of 5, 60 nm, respectively, at an interparticle distance of 4 nm. Spectra (d) and (f) were computed with spheres of 5, 60 nm, respectively, at an interparticle distance of 10 nm. The FDTD spectra were simulated with a mesh size of R/60. Figures (b) and (e) show the error scores for the IFA FDTD simulations with the FEM simulations taken as reference. Inserts in Figures (c) and (f) are computed with a R/100 mesh size.

distributed spheres. Very small interparticle distances may occur, and this is the scenario where IFA performs best.

3.3. Accuracy evaluation

The different structures have been simulated by the Finite Element Method with COMSOL. Accuracy evaluation of the FDTD simulations (with Per-C or IFA meshing) is performed by comparing them with FEM simulations (Fig. 7). For small nanoparticles (Fig. 7(a), 7(d)) and a mesh size of R/60 nm, both methods provide similar results. The peak positions (peaks of physical origin) are very similar and reported in Table 6. The differences lie in the peak intensities. The error score is below 1%, for the finest mesh, R/60, and a particle radius of 5 nm. These minor

differences mean that the same physical insights can be extracted from both methods. For larger particles, e.g. $R = 60$ nm, the error score lies within 1-3% for $R/60$ mesh size (Fig. 7(b), 7(e)). The associated spectra (Fig. 7(c), 7(f)) clearly show differences between FEM and FDTD results. In order to confirm that this is primarily due to a too coarse mesh size, a FDTD simulation with $R/100$ is shown as an insert; here an excellent agreement is reached between both methods. Figure 7(c) and 7(f) highlight also the benefit of employing IFA for coarser meshes. In particular, one can notice that the IFA-FDTD simulation is more accurate than the Per-C FDTD simulation (Fig. 7(c)) as the reflectance at 920 nm has a value of 63% for the FEM simulation, 58% for the IFA-FDTD simulation and only 49% for the per-C FDTD simulation. This also explains the positive value for F_{Δ}^{IFA} in Fig. 6. Moreover, a significant impact of IFA-FDTD, compared with Per-C FDTD, is visible in the 800-1000 nm region (Fig. 7(c)).

Table 6. Comparison of the reflection peak positions for IFA, Per-C FDTD and FEM simulations. Values obtained from Fig. 7

Interparticle distance (nm)	4		10	
	5	60	5	60
Radius (nm)				
FEM – peak position (nm)	900	830	900	810
IFA- peak position (nm)	912	836	944	819
Per-C - peak position (nm)	902	836	979	819

4. Discussion

In view of the results reported above, several published works, which make use of FDTD simulations for modelling plasmonic structures, are reviewed and discussed hereafter. Table 7 summarizes the most challenging values of 3 parameters (particle radius, interparticle distance, R/Δ) used in each reference. The last column indicates whether or not the convergence would be achieved if these parameters were used as input for our case study.

Table 7. The values of the 3 most critical parameters reported in each reference. The last column indicates whether or not the convergence would be achieved if these parameters were used as input for our case study. The most critical parameters for our work were determined by the intersection of the error curves with a threshold value of 1% in Fig. 7(b) and 7(e). R/Δ is the ratio between particle radius and mesh size.

TableReference	Software package	Radius (nm)	Interparticle distance (nm)	R/Δ	Nanoparticle pattern	Convergence (yes/no)
[31]	In-house FDTD	4	10.7	32	Periodic arrangement	yes
[24]	OmniSim package	12	10	3	Random distribution	yes/no
[30]	Lumerical	10	0.5	20	Chain-like structures	no
[57]	Lumerical	40	0.5	80	Dimers	no
[58]	MEEP	30	2	300	Dimers / trimers	yes
This work	In-house FDTD	5	10	27	Periodic arrangement	yes
This work	In-house FDTD	10	4	53	Periodic arrangement	yes

Lesina et al. used FDTD simulations to support their experimental bottom-up laser approach to form nanoparticles on a metallic surface through ablation and redeposition [31]. Various nanoparticle sizes were simulated. The smallest nanoparticle radius was 4 nm, with a mesh size

of 0.125 nm and the smallest interparticle distance was 10.7 nm. Those are the values we consider in Table 7 for this reference. In [31], it is stated that the chosen mesh size ensures converging results, which is confirmed by comparison with our results since we reach convergence for a mesh size of 0.250 nm in similar conditions.

Kozioł et al. investigated silver nanoparticles formed by thermal annealing of thin films. The lateral dimensions of their simulation domain was $2.7 \times 3.0 \mu\text{m}^2$ [24]. The positions and shapes of the nanoparticles followed experimental observations. The nanoparticle sizes followed a Gaussian distribution, and the smallest nanoparticle had a diameter of 12 nm. Due to the relatively large simulation domain, the mesh size was set to 12 nm (limited by the available computer memory). In their simulation geometry, the interparticle distance was most often about the size of the wavelength, and in some cases hotspots arose due to much smaller interparticle distances. It appears that, for an interparticle distance of 10 nm, their simulation grid was not fine enough. However, only few nanoparticles were both small and very close to one another. In most cases, the nanoparticles were much larger and far apart, and convergence was achieved according to our criteria. In Table 7, we therefore indicate “yes/no” in the last column.

Tira et al. used FDTD simulations to analyze the electromagnetic response of gold nanoparticles organized in chain-like structures [30]. They investigated the influence of the number of particles and the interparticle distance. The smallest interparticle distance was 0.5 nm and the nanoparticle radius was 10 nm. The authors reported that their simulations converged as the far-field response was identical to simulations with a 0.1 nm mesh size. However, a mesh of 0.5 nm means that there was only one Yee-cell between the nanoparticles. Our study clearly shows that this is a major cause of lack of convergence. This conclusion would not be different if silver would be replaced by gold in our study. Nonetheless, the chain-like structure is made of a finite number of particles, which is different from our periodic simulations, and might explain the discrepancy between both results.

Abu et al. studied the plasmon coupling, quantum yield and effect of tip geometry of gold nanoparticles using FDTD simulations [57]. They chose a mesh size of 0.5 nm and the nanoparticle dimers had a radius of 40 nm. The interparticle distance varied from 0.5 nm to 200 nm. Here again, the interparticle region was discretized using only one Yee-cell for the smallest interparticle distance. As a consequence, our study suggests some convergence issues may happen for such simulations. Again, the simulated structure consisted of dimers, which is different from a periodic structure.

Nagarajan et al. studied dimer and trimer nanosphere clusters and investigated the surface-enhanced Raman spectroscopic characteristics [58]. The silver nanoparticles had a radius of 30 nm and the interparticle distance was 2 nm. A very fine mesh of 0.1 nm was adopted in this study. Such a fine resolution ensures convergence even for a periodic arrangement like the one considered in this article. Despite the fact that in their study the interparticle distance was 4 times larger than in [30] and [57], the mesh size was much smaller.

5. Conclusion

We have studied the numerical convergence of FDTD method for plasmonic systems consisting of a periodic assembly of interacting spherical nanoparticles. The effect of the nanoparticle's radius and the interparticle distance were investigated as function of the mesh size and the effect of interface field averaging was examined. We showed that a fine meshing in the gap between the nanoparticles is essential for the convergence. Moreover, a fine resolution of the nanoparticle's surface (discretization error of curved surfaces using a cubic mesh) is equally important. To tackle the latter issue, we used IFA, which turned out to be essential for large nanoparticles (i.e., radius > 40 nm) in order to improve convergence. Finally, a good agreement between IFA FDTD and FEM was observed, which proves both techniques are well-suited for the simulation of this

kind of plasmonic structures. In literature, it frequently happens that articles do no mention any numerical parameters used in FDTD simulations.

Funding. Fonds De La Recherche Scientifique - FNRS (T.0166.20); Fonds pour la Formation à la Recherche dans l'Industrie et dans l'Agriculture.

Acknowledgments. This research used resources of the “Plateforme Technologique de Calcul Intensif (PTCI)” (<http://www.ptci.unamur.be>) located at the University of Namur, Belgium, which is supported by the FNRS-FRFC, the Walloon Region, and the University of Namur (Conventions No. 2.5020.11, GEQ U.G006.15, 1610468, RW/GEQ2016 et U.G011.22). The PTCI is member of the “Consortium des Équipements de Calcul Intensif (CÉCI)” (<http://www.ceci-hpc.be>).

Disclosures. The authors declare no conflicts of interest

Data availability. Data underlying the results presented in this paper are not publicly available at this time but may be obtained from the authors upon reasonable request.

References

1. Y. L. Wang, F. Nan, X. L. Liu, *et al.*, “Plasmon-enhanced light harvesting of chlorophylls on near-percolating silver films via one-photon anti-stokes upconversion,” *Sci. Rep.* **3**(1), 1861 (2013).
2. N. Zhou, V. López-Puente, Q. Wang, *et al.*, “Plasmon-enhanced light harvesting: applications in enhanced photocatalysis, photodynamic therapy and photovoltaics,” *RSC Adv.* **5**(37), 29076–29097 (2015).
3. S. Carretero-Palacios, A. Jiménez-Solano, and H. Míguez, “Plasmonic nanoparticles as light-harvesting enhancers in perovskite solar cells: a user’s guide,” *ACS Energy Lett.* **1**(1), 323–331 (2016).
4. J. N. Anker, W. P. Hall, O. Lyandres, *et al.*, “Biosensing with plasmonic nanosensors,” *Nat. Mater.* **7**(6), 442–453 (2008).
5. A. M. Shrivastav, U. Cvelbar, and I. Abdulhalim, “A comprehensive review on plasmonic-based biosensors used in viral diagnostics,” *Commun. Biol.* **4**(1), 70 (2021).
6. M. Kauranen and A. V. Zayats, “Nonlinear plasmonics,” *Nat. Photonics* **6**(11), 737–748 (2012).
7. N. C. Panoiu, E. I. Sha, D. Y. Lei, *et al.*, “Nonlinear optics in plasmonic nanostructures,” *J. Opt.* **20**(8), 083001 (2018).
8. E. Wagner Ferreira Sabará, V. Pereira, A. Luiz Molisani, *et al.*, “A review on the classification, characterisation, synthesis of nanoparticles and their application,” *IOP Conf. Ser.: Mater. Sci. Eng.* **263**(3), 032019 (2017).
9. E. Petryayeva and U. J. Krull, “Localized surface plasmon resonance: nanostructures, bioassays, and biosensing—a review,” *Anal. Chim. Acta.* **706**(1), 8–24 (2011).
10. Stefan A. Maier, *Plasmonics: Fundamentals and Applications* (Springer, 2007).
11. T. L. Temple and S. Dligatch, “Role of the spacer layer in plasmonic antireflection coatings comprised of gold or silver nanoparticles,” *J. Photonics Energy* **5**(1), 053095 (2015).
12. M. Rani, J. Kashyap, U. Singh, *et al.*, “Optimisation of dielectric spacer layer thickness in Ag nanospheres/ITO/c-Si structure for plasmonic solar cells using FDTD simulation,” *Mater. Technol.* **37**(10), 1320–1328 (2022).
13. A. Ahmed, G. Hajsalem, R. Gordon, *et al.*, “Plasmon hybridization for enhanced nonlinear optical response,” *Opt. Express* **20**(28), 29923–29930 (2012).
14. M. Hu, A. Ghoshal, M. Marquez, *et al.*, “Single particle spectroscopy study of metal-film-induced tuning of silver nanoparticle plasmon resonances,” *J. Phys. Chem. C* **114**(16), 7509–7514 (2010).
15. A. Said, K. S. R. Atia, and S. S. A. Obayya, “On modeling of plasmonic devices: overview,” *J. Opt. Soc. Am. B* **37**(11), A163–A174 (2020).
16. I. A. Fischer and J. Schlipf, “Rigorous coupled-wave analysis of a multi-layered plasmonic integrated refractive index sensor,” *Opt. Express* **29**(22), 36201–36210 (2021).
17. P. Sumithra and D. Thiripurasundari, “A review on computational electromagnetics methods,” *Advanced Electromagnetics* **6**(1), 42–55 (2017).
18. J. Feng and M. Santamouris, “Numerical techniques for electromagnetic simulation of daytime radiative cooling: A review,” *AIMS Mater. Sci.* **6**(6), 1049–1064 (2019).
19. Ya-Chi Liu, Kai Chang, John Fwu, *et al.*, “Performance comparison between FDTD and FEM for the simulation of plasmonic waveguide operating at optical communication frequency,” *USNC-URSI Radio Science Meeting* **1**, 184 (2013).
20. J. DE Rosenkrantz Lasson, L. Hagedorn Frandsen, P. Gutsche, *et al.*, “Benchmarking five numerical simulation techniques for computing resonance wavelengths and quality factors in photonic crystal membrane line defect cavities,” *Opt. Express* **26**(9), 11366–11392 (2018).
21. B. Gallinet, J. Jéf, J. Butet, *et al.*, “Numerical methods for nanophotonics: standard problems and future challenges,” *Laser Photonics Rev.* **9**(6), 577–603 (2015).
22. A. Sethi, M. Rafiee, S. Chandra, *et al.*, “A unified methodology for fabrication and quantification of gold nanorods, gold core silver shell nanocuboids and their polymer nanocomposites,” *Langmuir* **35**(40), 13011–13019 (2019).
23. Q. Wang, S. Zheng, Q. Shi, *et al.*, “Modified emission of polymer films by ultrathin Ag nanoparticle films,” *Vacuum* **157**, 111–114 (2018).

24. R. Kozioł, M. Łapiński, P. Syty, *et al.*, “Evolution of Ag nanostructures created from thin films: UV-vis absorption and its theoretical predictions,” *Beilstein J. Nanotechnol.* **11**, 494–507 (2020).
25. A. Yuksel, M. Cullinan, E. T. Yu, *et al.*, “Near-field plasmonics of gold nanoparticles in dielectric media,” *J. Quantum Spectrosc. Radiat. Transf.* **254**, 107207 (2020).
26. H. Li, Y. Hu, Y. Yang, *et al.*, “Theoretical investigation of broadband absorption enhancement in a-Si thin-film solar cell with nanoparticles,” *Solar Energy Mater. Solar Cells* **211**, 110529 (2020).
27. Y. F. C. Chau, C. T. C. Chao, H. P. Chiang, *et al.*, “Plasmonic effects in composite metal nanostructures for sensing applications,” *J. Nanopart. Res.* **20**(7), 190 (2018).
28. F. H. Saboor, S. Hadian-Ghazvini, and H. Heidarzadeh, “Design and performance simulation of a highly sensitive nano-biosensor based on a realistic array of plasmonic synthesized nanostructures,” *Photonics Nanostruct.* **49**, 100991 (2022).
29. S. Farooq, F. Wali, D. M. Zezell, *et al.*, “Optimizing and quantifying gold nanospheres based on LSPR label-free biosensor for dengue diagnosis,” *Polymers* **14**(8), 1592 (2022).
30. C. Tira, D. Tira, T. Simon, *et al.*, “Finite-difference time-domain (FDTD) design of gold nanoparticle chains with specific surface plasmon resonance,” *J. Mol. Struct.* **1072**(1), 137–143 (2014).
31. A. C. Lesina, J. M. Guay, A. Weck, *et al.*, “Modelling of coloured metal surfaces by plasmonics nanoparticles,” *NATO Science for Peace and Security Series B: Physics and Biophysics* **1**, 361–363 (2018).
32. G. A. E. Vandenbosch, M. Kupresak, V. V. Moshchalkov, *et al.*, “Benchmarking of software tools for the characterization of nanoparticles,” *Opt. Express* **25**(22), 26760–26780 (2017).
33. A. Taflov and S. C. Hagness, *Computational Electrodynamics: The Finite-Difference Time-Domain Method*, 3rd ed. (Artech House, n.d.).
34. K. S. Yee, “Numerical solution of initial boundary value problems involving Maxwell’s equations in isotropic media,” *IEEE Trans. Antennas Propagat.* **14**(3), 302–307 (1966).
35. A. Gansen, M. el Hachemi, S. Belouettar, *et al.*, “A 3D unstructured mesh FDTD scheme for EM modelling,” *Arch Computat. Methods Eng.* **28**(1), 181–213 (2021).
36. W. Yu, R. Mittra, D. Arakaki, *et al.*, “A conformal finite difference time domain technique for modeling curved dielectric surfaces,” *IEEE Microw. Wireless Compon. Lett.* **11**(1), 25–27 (2001).
37. W. Yu and R. Mittra, “A conformal FDTD algorithm for modeling perfectly conducting objects with curve-shaped surfaces and edges,” *Microw. Opt. Technol. Lett.* **27**(2), 136–138 (2000).
38. S. Dey and R. Mittra, “A locally conformal finite difference time domain technique for modeling arbitrary shaped objects,” *IEEE Antennas and Propagation Society International Symposium* **1**, 584–587 (1998).
39. S. Dey and R. Mittra, “A locally conformal finite difference time domain (FDTD) algorithm for modeling 3D objects with curved surfaces,” *IEEE Antennas and Propagation Society International Symposium* **4**, 2172 (1997).
40. S. Dey and R. Mittra, “A locally conformal finite difference time domain (FDTD) algorithm for modeling three dimensional perfectly conducting objects,” *IEEE Microw. Guid. Wave Lett.* **7**(9), 273–275 (1997).
41. L. L. L. Fortes and S. T. M. Gonçalves, “Wideband performance limitations of the C-FDTD in the discretization impoverishment of a curved surface,” *COMPEL - The international journal for computation and mathematics in electrical and electronic engineering* **39**(5), 1005–1015 (2020).
42. Lumerical, <https://www.lumerical.com/>
43. Lumerical, “Understanding Mesh Refinement and Conformal Mesh in FDTD,” <https://optics.ansys.com/hc/en-us/articles/360034382594-Understanding-Mesh-Refinement-and-Conformal-Mesh-in-FDTD>.
44. A. Lesina, A. Vaccari, P. Berini, *et al.*, “On the convergence and accuracy of the FDTD method for nanoplasmonics,” *Opt. Express* **23**(8), 10481–10497 (2015).
45. COMSOL Multiphysics, <https://www.comsol.com/>, COMSOL AB, Stockholm, Sweden (n.d.).
46. A. Stalmashonak, C. Matyssek, G. Seifert, *et al.*, “Comparison of numerical methods in near-field computation for metallic nanoparticles,” *Opt. Express* **19**(9), 8939–8953 (2011).
47. Y. He and T. Zeng, “First-principles study and model of dielectric functions of silver nanoparticles,” *J. Phys. Chem. C* **114**(42), 18023–18030 (2010).
48. J. Muller, G. Parent, S. Fumeron, *et al.*, “Near-field and far-field modeling of scattered surface waves. application to the apertureless scanning near-field optical microscopy,” *J. Quantum Spectrosc. Radiat. Transf.* **112**(7), 1162–1169 (2011).
49. G. Dai, L. Xu, K. Hahm, *et al.*, “Tip optimization for improvement of detection in scanning near-field optical microscopy,” *J. Opt.* **14**(7), 075703 (2012).
50. D. Lacroix, G. Jeandel, G. Parent, *et al.*, “Finite-difference time-domain and near-field-to-far-field transformation in the spectral domain: application to scattering objects with complex shapes in the vicinity of a semi-infinite dielectric medium,” *J. Opt. Soc. Am. A* **28**(5), 868–878 (2011).
51. L. Dagum and R. Menon, “OpenMP: an industry standard API for shared-memory programming,” *IEEE Comput. Sci. Eng.* **5**(1), 46–55 (1998).
52. A. Roden and S. Gedney, “Convolution PML (CPML): an efficient FDTD implementation of the CFS–PML for arbitrary media,” *Microw. Opt. Technol. Lett.* **27**(5), 334–339 (2000).
53. A. Deinega and S. John, “Effective optical response of silicon to sunlight in the finite-difference time-domain method,” *Opt. Lett.* **37**(1), 112–114 (2012).

54. A. P. Pérez-Marín, J. A. Aznárez, J. A. Méndez, *et al.*, “Self-consistent optical constants of SiC thin films,” *J. Opt. Soc. Am. A* **28**(11), 2340–2345 (2011).
55. A. Ciesielski, L. Skowronski, M. Trzcinski, *et al.*, “Controlling the optical parameters of self-assembled silver films with wetting layers and annealing,” *Appl Surf Sci* **421**, 349–356 (2017).
56. Refractive Index, <https://refractiveindex.info>.
57. A. S. M. Mohsin and M. B. Salim, “Probing the plasmon coupling, quantum yield, and effects of tip geometry of gold nanoparticle using analytical models and FDTD simulation,” *IEEE Photonics J.* **10**(3), 1–10 (2018).
58. A. Nagarajan, P. Aruna, Panchanathan, *et al.*, “FDTD study on evolution of trimer silver@silica nanospheres to dimer for SERS characteristics,” *Plasmonics* **17**(2), 647–652 (2022).